Research Article

Efficient 3-hydroxybutyrate production by quiescent *Escherichia coli* microbial cell factories is facilitated by indole-induced proteomic and metabolomic changes

Nicholas M. Thomson[1,6*]
Tomokazu Shirai[2]
Marco Chiapello[3]
Akihiko Kondo[2]
Krishna J. Mukherjee[4]
Easan Sivaniah[5]
Keiji Numata[1]
David K. Summers[6*]

[1]Enzyme Research Team, RIKEN Centre for Sustainable Resource Science, Wako-shi, Japan
[2]Cell Factory Research Team, RIKEN Centre for Sustainable Resource Science, Yokohama, Japan
[3]Cambridge Centre for Proteomics, University of Cambridge, Cambridge, UK
[4]School of Biotechnology, Jawaharlal Nehru University, New Delhi, India
[5]Institute for Integrated Cell-Material Sciences (iCeMS), Kyoto University, Kyoto, Japan
[6]Department of Genetics, University of Cambridge, Cambridge, UK

Correspondence: *Dr Nicholas M. Thomson and Dr David K. Summers, Department of Genetics, University of Cambridge, Downing Street, Cambridge, CB2 3EH, UK.
E-mail: nthomson@cantab.net; dks11@cam.ac.uk

Keywords: Cell factory; *Escherichia coli*; Indole; Quiescence; 3-hydroxybutyrate

Abbreviations: PPP, pentose phosphate pathway; **TCA cycle**, tricarboxylic acid cycle; **Q-cells**, quiescent cell expression system; **H-NS**, histone-like nucleoid structuring protein; **PMF**, proton-motive force; **3HB**, 3-hydroxybutyrate; **Ac-CoA**, acetyl-coenzyme A; **2d-DIGE**, 2-dimensional differential in-gel electrophoresis; **LC-MS/MS**, liquid chromatography – tandem mass spectrometry; **HPLC**, high performance liquid chromatography; **MEBA**, multivariate empirical Bayes analysis for time-course data; **PEP**, phosphoenolpyruvate; **ROS**, reactive oxygen species

Abstract

We show here that quiescent (Q-Cell) *Escherichia coli* cultures can maintain metabolic activity in the absence of growth for up to 24 h, leading to four times greater specific productivity of a model metabolite, 3-hydroxybutyrate (3HB), than a control. Q-cells can be created by using the proton ionophore indole to halt cell division of an *hns* mutant strain. This uncouples metabolism from cell growth and allows for more efficient use of carbon feedstocks because less metabolic effort is diverted to surplus biomass production. However, the reason for the increased productivity of cells in the quiescent state was previously unknown. In this study, proteome expression patterns between wild-type and Q-cell cultures show that Q-cells overexpress stress response proteins, which prime them to tolerate the metabolic imbalances incurred through indole addition. Metabolomic data reveal the accumulation of acetyl-coenzyme A and phosphoenolpyruvate: excellent starting points for high-value chemical production. We demonstrated the exploitation of these accumulated metabolites by engineering a simple pathway for 3HB production from acetyl-coenzyme A. Quiescent cultures produced half the cell biomass of control cultures lacking indole, but were still able to produce 39.4 g L^{-1} of 3HB compared to 18.6 g L^{-1} in the control. Q-cells therefore have great potential as a platform technology for the efficient production of a wide range of commodity and high value chemicals.

1 Introduction

The bacterium *Escherichia coli* offers abundant opportunities for use as a cell factory for the commercial scale production of high value or commodity chemicals from cheap, renewable feedstocks [1–4]. In *E. coli* and other microbes, carbon flux through the central carbon metabolism pathways of glycolysis, the pentose phosphate pathway (PPP) and the tricarboxylic acid cycle (TCA) is at a maximum during exponential growth [5]. Consequently, microbe-based bioproduction processes usually aim to extend the exponential phase for as long as possible before nutrient limitation, oxygen deprivation or the accumulation of toxic by-products inhibit further carbon metabolism and cell growth [6–8]. Consequentially, large amounts of biomass are generated by this strategy. To generate biomass requires the diversion of chemical feedstocks for maintenance of cell function and production of essential macromolecules [9], thereby reducing the yield of the intended product. High cell density batch production also poses significant engineering challenges to increase nutrient and oxygen uptake rates, provide sufficient mixing and cooling, and to separate product efficiently from the accumulated biomass.

Continuous production using a chemostat solves some of these problems by removing cells at the same rate as they are produced by division [10, 11]. In some situations it is also possible to use 'resting cells' in an osmotically-balanced but nutrient-limited buffer such as phosphate buffered saline [12, 13]. However, these approaches are technically more challenging and suffer from problems including vulnerability to contamination in chemostats and limited viable lifespans of resting cells.

The non-growing but metabolically active quiescent cell expression system (Q-cells) diverts resources away from unwanted biomass accumulation and towards product formation [14]. Quiescence is achieved by addition of 2.5 – 3.0 mM indole to cultures of *E.*

coli W3110 carrying a stop codon after the 93rd codon of the *hns* gene (*hns*Δ93). This mutation causes the production of a truncated Histone-like Nucleoid Structuring protein (H-NS). After indole is added, metabolic activity continues and production of plasmid-encoded proteins is increased, but only in *hns* mutants [15, 16]. Indole is a well-studied chemical signal in over 85 species of bacteria [17]. It is a proton ionophore and has been shown to reduce the proton-motive force (PMF) of *E. coli* by allowing protons to return to the cytoplasm after their expulsion to the periplasmic space during oxidative phosphorylation [18]. One effect of reducing the PMF is to prevent the formation of the FtsZ ring, which is a prerequisite for cell division. Therefore, at suitable concentrations indole is able to prevent *E. coli* cell division [19].

Q-cells have previously only been investigated for the production of proteins [16]. Here, we demonstrate the potential for using Q-cells to synthesise a wide and diverse range of industrially-relevant small molecules under fed-batch conditions. Using metabolomic and proteomic approaches, we move towards a greater understanding of the mechanisms underlying the quiescent state. We also show that quiescent cells accumulate a large reservoir of acetyl-coenzymeA (Ac-CoA). To demonstrate the tractability of the system, we designed a simple fermentation strategy for improved production of 3-hydroxybutyrate (3HB) from Ac-CoA.

2 Materials and methods

2.1 Strains and growth conditions. The wild-type strain used as the control was *E. coli* W3110 (ATCC 27325). To create the Q-cell strain, the *hns*Δ93 mutation was introduced to the wild-type strain using the lambda Red recombinase system, as described previously [15]. Strains were stored with glycerol at -80 °C and streaked onto Luria-Bertani (LB) agar plates before use. A 5 ml starter culture was then grown in LB liquid medium for 8 h at 37

°C and used to inoculate further cultures for the experiments. The *hns*Δ93 mutation confers kanamycin resistance to the Q-cell strain. For selection purposes, Q-cell plates and starter cultures contained kanamycin (30 μg mL^{-1}). However, to keep the conditions used for each strain as similar as possible, no antibiotics were used for experimental cultures, except when necessary for maintenance of the 3HB production plasmid.

For the metabolome and proteome studies, cultures were grown in M9 medium (12.8 g L^{-1} $Na_2HPO_4.7H_2O$, 3 g L^{-1} KH_2PO_4, 0.5 g L^{-1} NaCl, 1 g L^{-1} NH_4Cl and 0.24 g L^{-1} $MgSO_4$) supplemented with 4 g L^{-1} glucose, 2 g L^{-1} yeast extract and 1 ml.L^{-1} of a trace elements solution (9.7 g L^{-1} $FeCl_3$, 7.8 g L^{-1} $CaCl_2$, 0.218 g L^{-1} $CoCl_2.6H_2O$, 0.156 g L^{-1} $CuSO_4.5H_2O$, 0.118 g L^{-1} $NiCl_3.6H_2O$ and 0.105 g L^{-1} $CrCl_3.6H_2O$ dissolved in 0.1 M HCl). Seed cultures (300 mL) were inoculated with 3 mL of LB starter culture in 1 L baffled Erlenmeyer flasks and grown for 16 h overnight with shaking at 300 rpm.

Following inoculation of the fermentor (final volume of 3 L in a 10 L vessel), cultures were grown in batch mode until the glucose supply was exhausted, indicated by a rise in dissolved oxygen (DO) and pH, and confirmed by testing with a hand-held FreeStyle Optium glucose meter (Abbott Laboratories, UK). Feed solution (180 g L^{-1} glucose, 22 g L^{-1} NH_4Cl, 5.42 g L^{-1} $MgSO_4$) was then introduced at 1.5 mL min^{-1} by peristaltic pump. Throughout the experiment, the temperature was controlled at 37 °C, agitation speed was a constant 500 rpm (sufficient to maintain DO above 40 %) and pH was maintained at 7.0 by addition of 5 M NaOH as necessary. Control of foaming was only necessary for wild-type cultures without indole, and was achieved by automatic addition of antifoam agent A (Sigma-Aldrich, US) controlled by a foam level probe.

After a 30 min equilibration period, indole dissolved in ethanol (1 M) was added in a single shot to a final concentration of 3 mM. An equivalent volume of pure ethanol was added for no-indole controls. The growth of each culture was monitored by measuring the optical density at 600 nm (OD_{600}) of samples. Although the growth rates differed between strains, the OD_{600} at the start of the feeding stage was the same for all cultures.

For the production of 3HB, a similar strategy was followed to that described above. However, a complex medium could be used as it was no longer necessary to avoid activating alternative metabolic pathways, as in the metabolome study. This also allowed both strains to grow at equal rates. We used terrific broth (TB) at all stages of the 3HB production experiments. TB medium consists of 24 g L^{-1} yeast extract, 12 g L^{-1} peptone, 9.4 g L^{-1} K_2HPO_4, 2.2 g L^{-1} KH_2PO_4, 4 g L^{-1} glucose and 2.4 g L^{-1} $MgSO_4$. A 100 mL pre-culture of *E. coli* W3110*hns*Δ93/pTrctesBphaAB was grown overnight in TB medium at 37 °C then used to inoculate the fermentor (5 L vessel), which contained a further 1.9 L of fresh TB medium. Ampicillin (100 μg/mL) was included in all growth media and the nutrient feed, to select for cells containing the plasmid.

When the original glucose supply was depleted (signaled by a rise in pH), a feed medium consisting of 190 g L^{-1} glucose, 108 g L^{-1} peptone, 84 g L^{-1} yeast extract, 9.4 g L^{-1} K_2HPO_4, 2.2 g L^{-1} KH_2PO_4 and 1.2 g L^{-1} $MgSO_4$ was pumped into the fermentor at an initial flow rate of 0.28 mL min^{-1}. The ratio of glucose to complex nitrogen in this feed was kept much higher than TB medium to provide a better stoichiometric balance. The flow rate was increased exponentially so as to double every 2 h pre-induction to keep pace with the growth rate of the cells. Indole was dissolved in ethanol to 150 mM and pumped into the fermentor at a rate of 0.28 mL min^{-1} for 2 h, through a tube that exited below the level of the medium to ensure good dissolution. Induction was done with IPTG (1 mM final

concentration) 30 min after the start of the indole feed. The feed rate post induction was kept constant since we observed a drop in the growth rate of the cells.

Cell growth was measured as OD_{600} following appropriate dilution and as cell dry weight (CDW) by collecting the cells from two 1 mL samples through centrifugation and drying in an oven until constant weight. The average of the two weights was reported. Glucose concentrations were recorded using a medical glucose meter and disposable enzyme assay strips. Substrate consumption rates (with respect to glucose) were calculated from a material balance on the amount fed per unit time and the residual glucose concentration in the culture medium. Following centrifugation at 17,000 × g for 2 minutes to remove the cells, samples of the supernatant (1 mL) were kept at -80 °C before testing for 3HB concentrations using a *β*-hydroxybutyrate colorimetric assay kit (Cayman Chemicals, US).

2.2 3-hydroxybutyrate production plasmid construction. Plasmid pTrctesBphaAB was constructed from plasmid pTrcphaCAB$_{Re}$ which was generously provided by Dr. Takeharu Tsuge (Tokyo Institute of Technology, Japan) [20], by replacing the *phaC* gene with *tesB*. The artificial operon thus created encoded for a 3-enzyme pathway in which 3-hydroxybutyryl-CoA is produced from Ac-CoA by PhaA and PhaB, and the CoA moiety is then removed by TesB to leave 3-HB. The *tesB* gene was amplified by PCR from plasmid pCA24N:TesB [21] and the product was purified using a QIAQuick PCR purification column (Qiagen, USA). Plasmid pTrcphaCAB$_{Re}$ was linearised by digestion with EcoRI and SalI and the plasmid backbone was then ligated with the *tesB* fragment by Gibson Assembly according to the manufacturer's instructions of a kit provided by New England Biolabs (US). The primers used for Gibson Assembly were:

Forward: 5'-AACAATTTCACACAGGAAACAGACCATGGAATTCAGATCTTTCG

AATAGTGACGGCAGAGAGACAATCAAATCATG-3’

Reverse: 5’-CAAAACAGCCAAGCTTGCATGCCTGCAGGTCGACTCTAGAGGAT CCAAACCCGGTGAATTGGCGCA-3’

2.3 Time-course study of metabolomics changes. Samples were taken immediately before indole addition and at six other points over the next 4 hours (5, 15, 30, 60, 120 and 240 min after indole addition). Approximately 20 mL samples were drawn aseptically from the fermentor, 1 mL aliquots of which were used for the metabolomics study. The OD_{600} of each sample was measured with appropriate dilution and recorded, and later used to normalise the metabolite concentrations. We obtained samples for metabolite quantification by vacuum filtering 1 mL of each culture and quenching the cells by immersion in cold (-80 °C) methanol within 30 sec of withdrawal. The samples were stored in methanol at -80 °C until preparation for analysis.

2.4 LC-MS/MS analysis of metabolites. Prior to analysis, metabolites were extracted using a previously described method with modifications [22, 23]. Briefly, the metabolites were extracted into a 1.2 ml solvent mixture ($CHCl_3$:H_2O, 1:1, v/v) containing 10 μg L^{-1} of D-(+)-camphor-10-sulfonic acid as an internal standard for semi-quantitative analysis. After centrifugation at 15,000 × g at 4 °C for 5 min, 10 μL of the upper phase was used for quantification of intracellular metabolites by high-performance liquid chromatography coupled with electrospray ionisation tandem mass spectrometry (LCMS-8040 triple quadrupole LC-MS/MS spectrometer; Shimadzu, Japan) as described previously [24].

2.5 GC-MS analysis of metabolites. For GC-MS analysis, 70 μL of the upper phase, as for LC-MS/MS analysis, was transferred to a new tube and vacuum dried. The dried residue

was derivatised for 90 min at 30 °C in 20 mg mL^{-1} methoxyamine hydrochloride in pyridine (20 μL). Subsequently, trimethylsilylation (TMS derivatisation) was performed for 30 min at 37 °C and then for 2 h at room temperature with N-methyl-N-(trimethylsilyl)trifluoroacetamide (MSTFA, 50 μL) [25, 26]. GC-MS was carried out using a GCMS-QP2010 Ultra (Shimadzu, Japan) equipped with a CP-Sil 8 CB-MS capillary column (30 m × 0.25 mm × 0.25 μm; Agilent, USA). Helium was used as the carrier gas with a flow rate of 2.1 mL min^{-1}. The injection volume was 1 μL with a split ratio of 1:10. An initial oven temperature of 60°C was maintained for 10 min, then raised to 315 °C at 15 °C min^{-1}, and maintained for 6 min. The total running time was 33 min. The other settings were as follows: 250 °C interface temperature, 200 °C ion source temperature, and electron impact (EI) ionisation at 70 eV.

2.6 ^{13}C metabolic flux analysis. Cells were harvested in the logarithmic growth phase by centrifugation and then hydrolysed in 5 M HCl at 100 °C for 20 h. Amino acids were purified and evaporated as previously described [27], and then derivatised prior to their analysis by GC-MS, as previously described [28] The flux distribution ratio between glycolysis and the PPP was determined as previously described [29]. Briefly, almost all mass isotopomer fractions, especially serine, glycine, and alanine, show significant variations depending on the distribution ratio. In this study, [1-^{13}C] labeled glucose was used to analyse that ratio. Lower proportions of the m1 fractions of the above amino acids are seen by GC-MS at higher PPP fluxes. This is due to the loss of labeled C1 in the decarboxylation reaction of the oxidative PPP. That is, labeled carbon atoms can exit only through glycolysis. Therefore, the split ratio of glycolysis can be determined by dividing the labeled mass fractions of serine, glycine and alanine by the unlabeled fraction.

2.7 HPLC analysis for measurement of organic acids in medium. Supernatant of the cell broth, recovered after centrifugation, was used for HPLC using a Prominence HPLC System (Shimadzu, Japan) with a conductivity detector and two Shim-pack SCR-102H columns (300 mm x 8.0 mm; I.D., 7 μm; Shimadzu, Japan). The column temperature was 48 °C and the flow rate of the mobile phase (5 mM p-toluenesulfonic acid; p-TSA) was 0.8 mL min^{-1}. The flow rate of the pH buffering solution for the detector (5 mM p-TSA, 20 mM Bis-Tris, and 0.1 mM EDTA-4H) was 0.5 mL min^{-1}.

2.8 2d-DIGE comparison of protein expression. The same 20 mL samples from the fermentation cultures as described for the metabolomics study were used for the proteomic study. A 10 mL aliquot of each sample was centrifuged at 4000 × g for 15 min to recover the cells. The pellet was then washed 3 times by repeated suspension and centrifugation, in an ice-cold buffer consisting of 10 mM Tris (pH 8.0) and 5 mM magnesium acetate. Washed pellets were stored at -80 °C until all samples had been collected, and then prepared for analysis simultaneously.

Cells were resuspended in lysis buffer (7 M urea, 2 M thiourea, 30 mM Tris and 4% (w/v) CHAPS) and lysed by sonication on ice. The sonication protocol consisted of 12 cycles of 10 sec with 10 sec rest periods between. The pulse amplitude was set to 15 Amp resulting in a pulse power of 8 – 9 W. After complete lysis, the protein concentration was measured using a Bradford microplate assay procedure. Controls consisting of bovine serum albumin were prepared in the same lysis buffer to prepare a standard curve. The pH of each sample was also checked and found to be close to pH 8.5, which is optimal for the labelling procedure.

An internal standard was created by pooling equal amounts of protein from every sample. For the test samples, 50 μg of protein was labelled for each sample. Labelling was carried out with the CyDye DIGE Fluor minimal labelling kit (GE Healthcare, US) using Cy2 for the internal standard and Cy3 and Cy5 for test samples. Groups of two test samples were then combined together with an internal standard sample, and mixed with an equal volume of 2× sample buffer (7M urea, 2 M thiourea, 2% (w/v) CHAPS, 0.5% IPG buffer (pH 3 – 11 NL) and De-streak reagent). Finally, the volume was made up to 450 μL with rehydration solution (7 M urea, 2 M thiourea, 2% (w/v) CHAPS). Each sample was loaded onto a 24 cm Immobiline DryStrip (pH 3 – 11 NL) using the rehydration method, with rehydration proceeding for 12 h at 20 °C. Isoelectric focusing then proceeded with an initial step of 500 mV for 1 h, followed by a gradient to 100 mV over 8 h, a gradient to 8000 mV over 3 h and a final step with the voltage held at 8000 mV for 3.75 h.

The second-dimension electrophoresis was conducted using the Ettan DALT gel and electrophoresis system (GE Healthcare, USA). 24 cm pre-casted gels were used following equilibration of the focused IEF strips. 8 gels were run simultaneously with 12 mA per gel, with a recirculating pump and chiller to maintain the buffer temperature at 15 °C, for 17 h until the bromophenol blue dye front just reached the end of the gel. The gels were then immediately scanned using a Typhoon 9400 variable mode imager (Amersham Biosciences, UK) and following the manufacturer's recommended settings. The images were analysed to detect changes in protein concentrations using DeCyder 2-D v.6.5 image analysis software.

2.9 Protein digestion and identification. A preparatory gel containing 500 μg of unlabeled, pooled samples was run under the same conditions as for the analytical gel, and post-stained using SYPRO Ruby (Fisher Scientific, Japan). Following spot matching in

DeCyder 2-D, the selected spots were excised using an Ettan spot picker (Amersham Biosciences, UK). The spots were de-stained in 50 mM ammonium bicarbonate containing 50% acetonitrile (50 µL) for 10 min at 37 °C, dehydrated with acetonitrile (25 µL) then dried in a vacuum centrifuge. To reduce cysteine residues, 100 mM ammonium bicarbonate with 10 mM dithiothreitol (25 µL) was added for 15 min at 50 °C, then 250 mM iodoacetamide in 100 mM ammonium bicarbonate (2 µL) was then added and the spots were incubated for 15 min at room temperature in the dark for alkylation. After washing and dehydration as before, the protein in the dried gel debris was digested at 37 °C overnight with 100 ng/10 µL modified trypsin solution. The digested protein fragments were collected from the supernatant and extracted from the gel debris by the addition of 50-80% acetonitrile containing 1% trifluoroacetic acid (3 × 25 µL).

The resulting protein sample was resolved in 2% acetonitrile containing 0.1% trifluoroacetic acid and applied to the liquid chromatography (LC) system (Advance nanoLC; Bruker-Michrom, USA) coupled to an LTQ linear ion trap mass spectrometer (ThermoFisher, USA) with a nanospray ion source in positive mode. The peptides were separated on a NANO-HPLC C18 capillary column (0.075 mm ID × 150 mm length, 3 mm particle size; Nikkyo Technos, Japan) using a linear gradient (25 min, 5-35% acetonitrile containing 0.1% formic acid) at a flow rate of 300 nL/min. The LTQ-MS was operated in top-3 data-dependent scan mode. The precursor ions were selected automatically for MS/MS analysis on the basis of their signal intensities. The parameters of LTQ were as follows: spray voltage, 2.3 kV; capillary temperature, 250 °C; mass range (m/z), 400-1800; collision energy, 35%. Raw data was acquired by Xcalibur software. The MS/MS data were searched against the SwissProt 2014_10 database using MASCOT v.2.4.1 software (Matrix Science, UK). The MASCOT search parameters were as follows: enzyme, trypsin; fixed modifications, carbamidomethyl (Cys); variable modifications, oxidation (Met); peptide

mass tolerance, ± 1.5 Da; fragment mass tolerance, ± 0.8 Da; max. missed cleavages, 1. Significant MASCOT scores were defined with $p \leq 0.05$.

2.10 Data analysis

Data pre-treatment and MEBA were done in Microsoft Excel and using an online user interface for metabolomics data analysis in R, MetaboAnalyst 3.0 [30]. Pre-treatment involved grouping all data by growth condition, normalising concentrations by the OD_{600} at which the sample was taken, then centering and Pareto scaling to generate relative concentration changes. All other statistical analyses were performed in R, and graphs were produced in R and Origin 8.0 (OriginLab, USA).

3 Results

We grew the wild-type and *hns*Δ93 mutant strain of *E. coli* W3110 in 3 L aerobic, fed-batch fermentations with or without the addition of indole. The *hns*Δ93 cultures grew slower than the wild-type (Fig. 1A). Therefore, we normalised the early culture conditions by inoculating into modified mineral salts medium (M9GYT) containing 0.4% glucose, 0.2% yeast extract and trace elements, and growing until the initial carbon supply was exhausted. At this stage, every culture reached the same optical density at 600 nm (OD_{600}; overall average 6.69, standard deviation 0.48). The nutrient feed was then started and quiescence was induced 30 min later by addition of indole (final concentration of 3 mM from a 1 M stock dissolved in ethanol) or an equivalent volume of pure ethanol. Only *hns*Δ93 cultures entered quiescence, whereas wild-type growth was inhibited but not stopped by indole.

3.1 Global protein expression changes are primarily due to the *hns* mutation

We hypothesised that the signaling and protonophore effects of indole would lead to widespread, significant changes in protein expression. However, since H-NS regulates approximately 5% of all gene expression in *E. coli* [31] we expected that the *hns*Δ93 mutation would also affect patterns of protein expression. To investigate these effects, we drew samples for protein expression profiling 1 h after the addition of indole. Surprisingly, 2-dimensional differential in-gel electrophoresis (2d-DIGE) showed that almost all the variation in protein expression was due to the strain genotype rather than indole addition (Fig. 1B), with distinct clusters formed by each strain (Fig. 1D). A total of 424 protein spots were present in every spot map (complete cases). Of the 303 spots that showed significant ($p \leq 0.05$) expression changes, 237 (78%) were due to only the strain and 27 (9%) were due to only indole addition (Fig. 1C). Using more stringent criteria, we identified 43 protein spots with ≥ 3-fold increase or decrease in expression compared to the control ($p \leq 0.001$). Analysis of variance (ANOVA) for the 43 selected spots showed that 39 spots varied due to the strain and 2 spots due to indole addition. The remaining 2 spots varied due to a combination of indole and strain, although there was no interaction.

The 43 selected spots were excised from the gel, digested by trypsin and subjected to peptide fingerprinting analysis via mass spectrometry. The results were queried against the SwissProt database using MASCOT v.2.4.1, and we were able to identify 12 spots with a high certainty of representing a single protein (or, in one case, two) (Table 1). Of the 12 proteins identified, 8 are regulated by H-NS according to the Ecocyc database [32].Of these, 7 are involved in stress response functions and were up-regulated in the *hns*Δ93 strain. This suggests Q-cells might be 'primed' for metabolic stresses induced by indole addition to the medium. Interestingly, PyrB expression was reduced in *hns*Δ93. We noted earlier that the *hns*Δ93 mutant grew more slowly than the wild-type in mineral salts medium. PyrB knockout mutants are unable to grow in M9 medium due to a reduction in

nucleotide synthesis, so the reduction in PyrB expression in the mutant might explain its reduced growth rate in our experiment [33].

3.2 Indole and strain effects both contribute towards establishment of quiescence

We expected that by modifying the PMF indole would have widespread knock-on effects on central carbon metabolism. To investigate the extent of these effects and identify pathways that could be amenable to metabolic engineering, we conducted a time-course study over 240 min from the time of indole addition. We tracked the intracellular concentrations of 22 cofactors and intermediates of glycolysis and PPP using liquid chromatography – tandem mass spectrometry (LC–MS/MS), and 8 organic acids (pyruvate, lactate and intermediates of TCA) by gas chromatography – mass spectrometry (GC–MS). Glucose-ADP, isocitrate and NADH were removed from the analysis due to very low abundances. We also followed the extracellular concentrations of 6 organic acids by high performance liquid chromatography (HPLC). The quantitative (GC–MS and HPLC) and relative ratio (LC–MS/MS) concentrations for the 33 analysed species were normalised against the OD_{600} of the cultures at each time point. Results using each technology were then analysed in parallel, since direct comparisons between the two concentration reporting modes were not possible.

Metabolites tended to cluster with neighboring intermediates of their respective pathways (Fig. 2B, C), showing that any metabolic changes tended to affect whole pathways more than individual intermediates. Individual principal component analyses (PCA) for each time-point of the LC-MS/MS data revealed a dynamic interaction between the influences of strain differences and indole (Fig. 2D, Supplementary Fig. 1). Before indole addition, the samples were relatively closely clustered with some separation by strain along principal

component (PC) 1 (accounting for 56% of the observed difference). Within 5 min of indole addition, indole treatment became the dominant clustering factor, while PC1 became less important (38.3% of observed differences). The influence of indole became more pronounced over the following 60 min, but by 240 min the samples tended to cluster more closely again, with some separation by strain. Untreated culture density was already high by this time and growth may have begun to slow. This suggests that the quiescent metabolic state resembles the late-logarithmic or early stationary phase of batch cultures. The GC-MS data revealed a similar trend for organic acids (Supplementary Fig. 2).

3.3 Indole causes re-routing of metabolic flow and pooling of metabolites from glycolysis in *hns*Δ93 cells

To identify the metabolites with the most significant changes in concentration during quiescence, we compared the time-courses of each intracellular metabolite between the control (wild-type, 0 mM indole) and quiescent cultures, and ranked them by the variation in time-course profile using Multivariate Empirical Bayes Analysis for time-course data (MEBA) [34]. Intermediates of PPP were unchanged or decreased in concentration over time under either condition (Table 2). However, glycolysis intermediates were present at higher concentrations in quiescent cells than in the control. We noted particularly significant increases in metabolites towards the later stages of glycolysis, namely phosphoenolpyruvate (PEP), 3-phosphoglycerate and 2-PG (3/2-PG), and Ac-CoA, of which the latter two increased over time in quiescent cells but decreased in the control. MEBA also revealed an effect of quiescence on the TCA cycle (Table 2). In control cultures, TCA intermediates slowly increased in concentration during growth. However, in quiescent cultures pyruvate and acids from the first half of TCA reduced in concentration, whereas those in the second half increased above the levels of the control. With the

simultaneous increase in Ac-CoA, this suggests indole inhibits the TCA cycle, possibly by preventing the conversion of Ac-CoA to citrate and/or altered regulation of the control point between PEP and pyruvate.

While MEBA only compared quiescent and control cultures, examination of the individual graphs of concentration versus time for each metabolite and cofactor under all four growth conditions (Supplementary Fig. 3 – 7) shows that indole alone had substantial effects on certain metabolite concentrations. Wild-type cells supplemented with indole rapidly built up large pools of F6P, G6P and Ac-CoA, exceeding the concentrations in quiescent cultures. However, the effect was short-lived and the concentrations rapidly decreased again after 120 min. In comparison, metabolic changes during the quiescent state appear generally to be more gradual and to endure for longer.

Supplementary Fig. 4 shows that wild-type cells had greater starting concentrations of PPP intermediates than *hns*Δ93. However, both strains had identical flux ratios through glycolysis, PPP and the Entner-Doudoroff pathway in ^{13}C-labelled chemostat experiments without indole (Supplementary Table 1). Due to its effect on growth, we could not investigate the changes in metabolic flux caused by indole. However, Fig. 2A, C and Table 2 both suggest that indole causes a non-H-NS dependent re-routing of metabolic flux away from the PPP.

HPLC measurements of the culture medium showed that acetate was the predominant extracellular carboxylic acid in all cultures. Formate was also produced in low concentrations, but pyruvate, lactate, succinate and fumarate were only detected in trace amounts (Supplementary Fig. 7). The kinetics of acetate production (Fig. 2B) suggested that in the absence of indole, the acetate switch mechanism [35] triggered acetate

accumulation as glucose became depleted at high culture densities. In the presence of indole, acetate was produced continually throughout the culture, reaching particularly high specific concentrations in quiescent cells. Thus, acetate production may have acted as an outlet for the glycolysis intermediates that accumulated due to the disruption of the TCA cycle.

A key function of the TCA cycle is to reduce NAD^+ to NADH, which acts as an electron donor for the electron transport chain. In our experiment, the concentrations of NAD^+ and the related molecule $NADP^+$ slowly decreased over 4 h under all conditions, but remained highest for *hns*Δ93 with 3 mM indole (Supplementary Fig. 6). The concentrations of the reduced forms of both molecules were also lower than the oxidised forms; in the case of NADH, below the limit of detection. Furthermore, concentrations of adenosine phosphates remained more constant in quiescent cultures than under other conditions. This supports the suggestion from the proteomics study that Q-cells are 'primed' for the metabolic stresses caused by indole, and so can maintain their redox balance even while experiencing shifts in metabolite concentrations.

3.4 Application of Q-cells to the production of 3-hydroxybutyrate

Our metabolomics analysis identified the potential for Q-cells to become efficient primary metabolite cell factories through targeted metabolic engineering using PEP or Ac-CoA as starting points. To test this principle, we chose 3HB as a model for metabolite production as it requires the expression of only three heterologous enzymes for its production from Ac-CoA and its presence in the growth medium can be assayed simply with commercially-available kits. To produce 3HB, two molecules of Ac-CoA are condensed by a *β*-ketothiolase (PhaA from *Cupriavidus necator*) and reduced at the *β*-position by an

acetoacetyl-CoA reductase (PhaB from *C. necator*), before the CoA moiety is removed by an overexpressed *E. coli* thioesterase B (TesB) [36, 37], as illustrated in Supplementary Fig. 8.

We introduced plasmid pTrctesBphaAB into *E. coli* W3110*hns*Δ93 to enable it to produce 3-hydroxybutyrate (3HB) in an IPTG-inducible manner. Terrific broth (TB) with glucose as the carbon source was chosen as the culture medium to avoid the slow growth of the *hns*Δ93 strain in M9GYT (Fig. 1A) [38]. Pilot experiments demonstrated that quiescence could be achieved with 2.5 mM indole so we used this concentration to minimise the potential for indole toxicity. After 26 h the quiescent culture reached an OD_{600} of 34.0, compared to 63.7 for a control culture with ethanol added in place of the indole solution (Fig. 4A). This corresponded to dry cell weights (DCW) of 13.3 g L^{-1} and 24.8 g L^{-1} respectively. Growth of the cultures was almost identical until indole addition, after which the Q-cell culture gradually ceased growing. Despite the reduced cell density, the 3HB concentration in the Q-cell culture reached 374.8 mM (39.4 g L^{-1}) at 26 h compared to 178.4 mM (18.6 g L^{-1}) for the control (Fig. 4B). Therefore, over the 26 h duration of the experiment, the specific productivity of the quiescent culture was 4.0-fold greater than for the control (0.114 against 0.029 $g_{product}$ g_{cells}^{-1} h^{-1}), while the absolute concentration in the culture supernatant was 2.1-fold greater.

Importantly, the rates of substrate (glucose, S) utilisation (dS/dt) were very similar for both cultures at all stages of the fermentation (Fig. 4C). On the other hand, the specific product (3HB, P) formation rates (given by 1/X(dP/dt), where X is biomass), representing the amount of 3HB produced per unit of time per unit of biomass, were initially similar but diverged 9 h into the experiment (Fig. 4D). Comparison with Fig. 4A demonstrates that the divergence corresponds with entry of the control culture into stationary phase. The abrupt halt in cell growth for the control culture was likely due to a combination of high cell

density and product inhibition caused by 3HB. Q-cells may be more tolerant of high 3HB concentrations due to not having a requirement for growth and division. 3HB production is linked to the metabolic rate of the cell. Therefore, the control culture became unproductive as metabolism slowed upon entry into stationary phase, whereas the quiescent culture continued to produce 3HB. It is this extended production period that accounts for the superior productivity of quiescent cultures. Ceasing growth clearly allows quiescent cultures to take advantage of the large pool of available metabolites that were revealed by our metabolomics analysis.

4 Discussion

We show here that the *hns*Δ93 mutation leads to wide-scale changes in protein expression and metabolite balance. Most significantly, stress response genes were upregulated, in agreement with previous characterisation of protein expression changes in an *hns* knockout strain [39]. Our results suggest that the *hns*Δ93 mutation essentially 'primes' cells for the effect of indole on metabolism and prepares the cells for quiescence. When indole is present, metabolism proceeds in a redox-imbalanced fashion, resulting in decreased NAD^+ and $NADP^+$ concentrations as the pathways that regenerate them are inhibited (Fig. 3). In the wild-type strain this soon leads to oxidative damage by reactive oxygen species (ROS) [40, 41]. However, in *hns*Δ93, elevated concentrations of stress-response proteins may enable the ROS to be neutralised, partly by oxidising NADH and NADPH. Therefore, the increased defense against oxidative stress in Q-cells may also act to regenerate cofactors, allowing for continued glucose metabolism. This model of indole action could shed further light on the metabolic shift that takes place as wild-type cells transition from exponential to stationary phase [42]. For example, it might be of benefit for cells to repress the TCA cycle when less energy is required to power cell growth and

division, and divert metabolic energy towards cell maintenance pathways leading from the PPP and glycolysis.

A comprehensive survey of protein expression changes due to indole has not been carried out in *E. coli*, but it has been suggested that proteins involved in drug and acid resistance [43–45], biofilm formation [46–48], amino acid metabolism [49], virulence [50], and even inter-species communication [17, 51] are all affected by indole. A microarray study of indole-induced expression changes in *Salmonella* found only 77 differentially expressed proteins [52]. Although we imposed more stringent cut-off parameters for the selection of significant expression changes, our results are in agreement that indole does not affect the expression of a large number of genes.

DNA replication and gene transcription in *E. coli* are coordinated throughout the growth cycle by controlling the topological structure of the chromosome [53–55]. It has also been suggested that a high density of DNA gyrase binding sites (and consequently high superhelical density) near to the replication origin is correlated with genes that are expressed early in the growth cycle [56, 57]. Indole inhibits DNA gyrase, but is not thought to have a strong effect at 3 mM [58]. Therefore, the protein expression and metabolic effects we observed are unlikely to be a consequence of DNA gyrase inhibition by indole. As noted before, other mutations in *hns* do not allow the induction of quiescence [14]. Therefore, we conclude that the *hns*Δ93 mutation affects the binding of H-NS to DNA in a way that loosens its control over the expression of a subset of the genes which it inhibits, and that this subset includes a large number of stress response genes.

It is not necessary for indole to affect protein expression in order to influence metabolite concentrations since metabolic balance is controlled largely through modulation of

enzyme activity [59]. Similarly, it is to be expected that the concentration changes we observed were relatively modest as *E. coli* is well evolved to maintain its metabolic balance under a wide variety of stressful conditions. Indeed, many metabolic engineering strategies fail due to the flexible *E. coli* metabolism finding 'work-arounds' through the expression of isozymes and the existence of alternative metabolic pathways [60]. While the most significant changes in this study were in the region between glycolysis and the TCA cycle, the data also indicate a general rapid decrease in PPP intermediates. The effect appears to be independent of the *hns*Δ93 mutation and may be due to an indole-mediated re-routing of metabolic flux away from the PPP. One might also expect that in the quiescent state, secondary pathways such as for amino acid, lipid and nucleic acid metabolism would also experience decreased flux due to lower demands from biomass production. However, further studies are required to confirm and characterise this inference.

As a protonophore, indole reduces the PMF, leading to increased proton pumping by the electron transfer chain [61]. This stimulates demand for NADH from the TCA cycle, leading to an increased rate of respiration. However, in our experiments the TCA cycle was disrupted by indole. Continued supply of glucose into glycolysis but reduced activity in the TCA cycle led to the build-up of glycolytic intermediates, particularly at the junction between glycolysis and the TCA cycle. It was recently reported that indole can increase anaerobic production of hydrogen and ethanol in a non-*hns*-mutant derivative of *E. coli* W3110 [62]. This intriguing result suggests that the accumulation of glycolysis products is also seen in anaerobic cultures exposed to indole. It would be interesting to compare the same strain under both aerobic and anaerobic conditions to compare the effects of indole and the strategies used by the cell to maintain redox balance.

As an example of the productive capacity of the Q-cell system we demonstrated enhanced production of 3HB. Other than adjusting the indole concentration, we made no attempt to optimise the production conditions. However, the 39.4 g L^{-1} of 3HB produced here was still greater than the highest previously reported concentration of 3HB of 12.2 g L^{-1} from 16.7 g L^{-1} DCW [36]. While indole induced a temporary 'burst' of Ac-CoA accumulation in wild-type cultures, only the maintenance of a (still increased, albeit smaller) pool of Ac-CoA seen in quiescent cultures could lead to the longer productive period and enhanced production seen here.

By better understanding the mechanism of entry into quiescence we have been able to identify promising starting points for metabolic engineering to improve the *hns*Δ93 strain for the production of commercially significant products through exploitation of the accumulated glycolysis intermediates. The uncoupling of production from biomass generation clearly leads to large increases in efficiency. Therefore, we believe that with additional metabolic engineering and optimisation of growth conditions, the Q-cell system will become a powerful and flexible tool for industrial-scale production of a variety of high value chemicals.

Acknowledgements

We would like to thank Dr Kenji Ohtawa (Riken Support Unit for Biomaterial Analysis, Japan) for technical assistance with 2D-DIGE, Dr Masaya Usui (Riken Support Unit for Biomaterial Analysis, Japan) for technical assistance with identification of protein spots, Dr Matthew Davey (Plant Sciences Department, University of Cambridge, UK) for helpful discussions about data analysis and Dr Antonio De León Rodríguez (IPICYT, Mexico) for critical reading of the manuscript. This project was funded by the Riken Foreign Postdoctoral Researcher program.

Conflict of interest

The authors declare no financial or commercial conflict of interest.

5 References

[1] C.D. Murphy, *Org. Biomol. Chem.* **2012**, *10*, 1949.
[2] C. Yu, Y. Cao, H. Zou, M. Xian, *Appl. Microbiol. Biotechnol.* **2011**, *89*, 573.
[3] Y. Li, *Protein Expr. Purif.* **2011**, *80*, 260.
[4] X. Chen, L. Zhou, K. Tian, A. Kumar, S. Singh, B.A. Prior, Z. Wang, *Biotechnol. Adv.* **2013**, *31*, 1200.
[5] S. Meier, P.R. Jensen, J.O. Duus, *FEBS Lett.* **2011**, *585*, 3133.
[6] S. Lee, *Trends Biotechnol.* **1996**, *14*, 98.
[7] A.B. Singh, A.K. Sharma, K.J. Mukherjee, *Mol. Biosyst. 8*, 615.
[8] J.H. Choi, K.C. Keum, S.Y. Lee, *Chem. Eng. Sci.* **2006**, *61*, 876.
[9] P. Van Bodegom, *Microb. Ecol.* **2007**, *53*, 513.
[10] P. a. Hoskisson, G. Hobbs, *Microbiology* **2005**, *151*, 3153.
[11] Q. Hua, C. Yang, T. Oshima, H. Mori, K. Shimizu, *Society* **2004**, *70*, 2354.
[12] H.J. Cha, R. Srivastava, V.N. Vakharia, G. Rao, W.E. Bentley, *Appl. Environ. Microbiol.* **1999**, *65*, 409.
[13] A. Ghazi, H. Therisod, E. Shechter, *J. Bacteriol.* **1983**, *154*, 92.
[14] D.C.D. Rowe, D.K. Summers, *Appl. Environ. Microbiol.* **1999**, *65*, 2710.
[15] C.-C. Chen, R. Walia, K.J. Mukherjee, S. Mahalik, D.K. Summers, *Biotechnol. J.* **2015**, *10*, 636.
[16] K.J. Mukherjee, D.C.D. Rowe, N.A. Watkins, D.K. Summers, *Appl. Environ. Microbiol.* **2004**, *70*, 3005.
[17] J.-H. Lee, J. Lee, *FEMS Microbiol. Rev.* **2010**, *34*, 426.
[18] C. Chimerel, A. Murray, E.R. Oldewurtel, D.K. Summers, U.F. Keyser, *ChemPhysChem* **2013**, *14*, 417.
[19] C. Chimerel, C.M. Field, S. Piñero-Fernandez, U.F. Keyser, D.K. Summers, *Biochim. Biophys. Acta* **2012**, *1818*, 1590.
[20] P. Kahar, J. Agus, Y. Kikkawa, K. Taguchi, Y. Doi, T. Tsuge, *Polym. Degrad. Stab.* **2005**, *87*, 161.
[21] M. Kitagawa, T. Ara, M. Arifuzzaman, T. Ioka-Nakamichi, E. Inamoto, H. Toyonaga, H. Mori, *DNA Res.* **2005**, *12*, 291.
[22] T. Soga, *Methods Mol. Biol.* **2007**, *358*, 129.
[23] S. Yoshida, J. Imoto, T. Minato, R. Oouchi, M. Sugihara, T. Imai, *Appl. Environ. Microbiol.* **2008**, *74*, 2787.
[24] B. Luo, K. Groenke, R. Takors, C. Wandrey, M. Oldiges, *J. Chromatogr. A* **2007**, *1147*, 153.
[25] U. Roessner, C. Wagner, J. Kopka, R. Trethewey, L. Willmitzer, *Plant J.* **2000**, *23*, 131.
[26] S. Strelkov, M. von Elstermann, D. Schomburg, *Biol. Chem.* **2004**, *385*, 853.
[27] A. Marx, A.A. de Graaf, W. Wiechert, L. Eggeling, H. Sahm, *Biotechnol. Bioeng.* **1996**, *49*, 111.
[28] T.P. Mawhinney, R.S. Robinett, A. Atalay, M.A. Madson, *J. Chromatogr.* **1986**, *358*, 231.
[29] M. Dauner, U. Sauer, *Biotechnol. Prog.* **2000**, *16*, 642.
[30] J. Xia, I. V. Sinelnikov, B. Han, D.S. Wishart, *Nucleic Acids Res.* **2015**, *43*, W251.
[31] F. Hommais, E. Krin, C. Laurent-Winter, O. Soutourina, A. Malpertuy, J. Le Caer, A. Danchin, P. Bertin, *Mol. Microbiol.* **2001**, *40*, 20.
[32] I.M. Keseler, J. Collado-Vides, A. Santos-Zavaleta, M. Peralta-Gil, S. Gama-Castro, L. Muniz-Rascado, C. Bonavides-Martinez, S. Paley, M. Krummenacker, T. Altman, P. Kaipa, A. Spaulding, J. Pacheco, M. Latendresse, C. Fulcher, M. Sarker, A.G. Shearer, A. Mackie, I. Paulsen, R.P. Gunsalus, P.D. Karp, *Nucleic Acids Res.* **2011**, *39*, 583.
[33] W.M. Patrick, E.M. Quandt, D.B. Swartzlander, I. Matsumura, *Mol. Biol. Evol.* **2007**, *24*, 2716.

[34] Y.C. Tai, T.P. Speed, *Ann. Stat.* **2006**, *34*, 2387.
[35] A.J. Wolfe, *Microbiol. Mol. Biol. Rev.* **2005**, *69*, 12.
[36] Q. Liu, S.-P. Ouyang, A. Chung, Q. Wu, G.-Q. Chen, *Appl. Microbiol. Biotechnol.* **2007**, *76*, 811.
[37] H.-C. Tseng, C.H. Martin, D.R. Nielsen, K.L.J. Prather, *Appl. Environ. Microbiol.* **2009**, *75*, 3137.
[38] K. Tartof, C. Hobbs, *Focus Life Technol.* **1987**, *9*, 10.
[39] C. Laurent-Winter, S. Ngo, A. Danchin, P. Bertin, *Eur J Biochem* **1997**, *244*, 767.
[40] A.R. Krapp, M.V. Humbert, N. Carrillo, *Microbiology* **2011**, *157*, 957.
[41] E. Cabiscol, J. Tamarit, J. Ros, *Int. Microbiol.* **2000**, *3*, 3.
[42] H. Gaimster, D. Summers, *PLoS One* **2015**, *10*, e0136691.
[43] H. Hirakawa, Y. Inazumi, T. Masaki, T. Hirata, A. Yamaguchi, *Mol. Microbiol.* **2005**, *55*, 1113.
[44] H.H. Lee, M.N. Molla, C.R. Cantor, J.J. Collins, *Nature* **2010**, *467*, 82.
[45] H. Hirakawa, M. Hayashi-Nishino, A. Yamaguchi, K. Nishino, *Microb. Pathog.* **2010**, *49*, 90.
[46] P. Di Martino, R. Fursy, L. Bret, B. Sundararaju, R.S. Phillips, *Can. J. Microbiol.* **2003**, *49*, 443.
[47] J. Lee, A. Jayaraman, T.K. Wood, *BMC Microbiol.* **2007**, *7*.
[48] T.K. Wood, *Environ. Microbiol.* **2009**, *11*, 1.
[49] D. Wang, X. Ding, P.N. Rather, *J. Bacteriol.* **2001**, *183*, 4210.
[50] H. Hirakawa, T. Kodama, A. Takumi-Kobayashi, T. Honda, A. Yamaguchi, *Microbiology* **2009**, *155*, 541.
[51] N.M. Vega, K.R. Allison, A.N. Samuels, M.S. Klempner, J.J. Collins, *Proc. Natl. Acad. Sci. U.S.A.* **2013**, *110*, 14420.
[52] E. Nikaido, E. Giraud, S. Baucheron, S. Yamasaki, A. Wiedemann, K. Okamoto, T. Takagi, A. Yamaguchi, A. Cloeckaert, K. Nishino, *Gut Pathog.* **2012**, *4*, 5.
[53] V.L. Balke, J.D. Gralla, *J. Bacteriol.* **1987**, *169*, 4499.
[54] L.S. Hsieh, R.M. Burger, K. Drlika, *J. Mol. Biol.* **1991**, *219*, 443.
[55] R.L. Ohniwa, K. Morikawa, J. Kim, T. Ohta, A. Ishihama, C. Wada, K. Takeyasu, *EMBO J.* **2006**, *25*, 5591.
[56] P. Sobetzko, A. Travers, G. Muskhelishvili, *Proc. Natl. Acad. Sci. U. S. A.* **2012**, *109*, E42.
[57] I.F. Lau, S.R. Filipe, B. Søballe, O.-A. Økstad, F.-X. Barre, D.J. Sherratt, *Mol. Microbiol.* **2004**, *49*, 731.
[58] C.M. Field, D.K. Summers, *Plasmid* **2012**, *67*, 88.
[59] N. Ishii, K. Nakahigashi, T. Baba, M. Robert, T. Soga, A. Kanai, T. Hirasawa, M. Naba, K. Hirai, A. Hoque, P.Y. Ho, Y. Kakazu, K. Sugawara, S. Igarashi, S. Harada, T. Masuda, N. Sugiyama, T. Togashi, M. Hasegawa, Y. Takai, K. Yugi, K. Arakawa, N. Iwata, Y. Toya, Y. Nakayama, T. Nishioka, K. Shimizu, H. Mori, M. Tomita, *Science* **2007**, *316*, 593.
[60] G. Unden, J. Bongaerts, *Biochim. Biophys. Acta - Bioenerg.* **1997**, *1320*, 217.
[61] S.S. Korshunov, V.P. Skulachev, A.A. Starkov, *FEBS Lett.* **1997**, *416*, 15.
[62] A. De Leon-Rodriguez, S.L. Caño-Muñiz, J. Liu, D.K. Summers, *N. Biotechnol.* **2016**, *33*, 868.

Table 1. Identities and properties of proteins with greater than 3-fold change in concentration from the control and p < 0.001. Proteins extracted from cells gown under all four conditions were separated on a series of 2d-DIGE gels as described in the text. Significant differences in expression were identified using DeCyder 2-D software, and the relevant spots were excised, digested and identified by LC-MS/MS.

Spot ID[a]	Protein Name	Gene	Theoretical M_r	Fold Change[b]	Change due to:	Pathway / function
877	NADP+-specific glutamate dehydrogenase	*gdhA*	48,778	-4.14	Strain	Glutamate synthesis
1319	Aspartate carbamoyltransferase	*pyrB*	34,463	-6.23	Strain	Pyrimidine nucleotide synthesis
1932	Protein YciF	*yciF*	18,643	14.90	Strain	Osmotic shock
1988	Aspartate carbamoyltransferase regulatory chain	*pyrI*	17,338	-4.59	Strain	Regulatory partner of PyrB
2090	Protein YciE	*yciE*	19,007	14.67	Strain	Osmotic shock
2050	DNA protection during starvation protein	*dps*	18,684	5.82	Strain	DNA protection
2121	50S ribosomal protein L10	*rlpJ*	17,757	6.94	Strain	Ribosome component
2145	Uncharacterised protein YgaU	*ygaU*	16,053	3.68	Strain	Osmotic shock
2153	Peroxiredoxin	*osmC*	15,193	4.70	Strain	Oxidative stress
2235	1) 50S Ribosomal protein L9 2) Outer membrane assembly factor	1) *rplI* 2) *bamE*	1) 12,149 2) 12,408	3.40	Indole	1) Ribosome component 2) Unknown
2314	Thioredoxin-1	*trxA*	11,913	3.25	Strain	Control of redox potential
2375	Protein YjbJ	*yjbJ*	8,320	8.90	Strain	Osmotic shock

[a] Underlined ID numbers indicate proteins regulated by H-NS

[b] Average fold change in expression level (n = 4) 1 h into the time-course experiment. Positive numbers represent increased concentration and negative numbers represent a decrease.

Table 2. Most significantly changed metabolites during the time-course experiment. Metabolites were extracted and quantified by LC-MS/MS or GC/MS as described in the text. Significant differences in time-course concentration profiles were detected using the MEBA module in MetaboAnalyst 3.0 [27].

Metabolite	Pathway	Fold change in WT, 0 mM	Fold change in hnsΔ93, 3 mM	Hotelling T^2
LC-MS/MS				
Phosphoenolpyruvate	Glycolysis	1.13	2.91	87.62
Sedoheptulose-7-P	PPP	-1.03	-1.23	58.72
NAD^+	Cofactor	-1.48	-1.28	53.53
Fructose-1,6-BP	Glycolysis	-1.65	-1.30	50.44
3/2-phosphoglycerate	Glycolysis	-1.01	1.53	48.97
ADP	Cofactor	-1.28	1.09	48.66
Acetyl-CoA	Glycolysis/TCA	-1.27	1.41	42.27
Ribose-5-P	PPP	-2.56	-1.38	35.69
Xylulose-5-P	PPP	-1.76	-1.70	34.58
Ribulose-5-P	PPP	-1.35	-1.76	33.05
GC-MS				
α-ketoglutarate	TCA	-1.13	-1.52	95.42
Malate	TCA	1.03	2.00	73.18
Succinate	TCA	1.72	2.06	72.79
Fumarate	TCA	1.16	1.74	70.56
Citrate	TCA	1.23	-2.81	64.18
Pyruvate	Glycolysis/TCA	1.64	-1.63	49.01
Lactate	Other	1.57	-1.51	42.51

Figure legends

Figure 1. Global changes in protein expression in quiescent cultures. a, Growth curves of each strain during the time-course experiment. The inset graph shows a magnified area of the same data from the time feeding was started until 30 mins into the time-course. Error bars represent the standard deviations (n = 4). **b**, Principal component analysis on the protein expression data confirms a single principal component accounted for the majority of variation, with clear separation by strain. **c**, Significantly up- and down-regulated proteins from the complete cases, grouped by the cause(s) of the change in expression, as determined by ANOVA ($p < 0.05$). **d**, Heat map of fold-changes in protein expression determined by 2d-DIGE for 424 complete cases.

Figure 2. Changes in metabolite concentration during the time-course. **a**, Heat map of concentration changes in cofactors and intermediates of glycolysis and PPP analysed by LC-MS/MS. **b**, Heat map of concentration changes in intermediates of the TCA cycle plus pyruvate and lactate, analysed by GC-MS. **c**, Accumulation of acetate in the culture medium for each condition tested. Error bars represent standard error (n = 4). Abbreviations for metabolite names: S7P, sedoheptulose-7-phosphate; Ribu5P, ribulose-5-phosphate; Rib5P, ribose-5-phosphate; X5P, xylulose-5-phosphate; G3P, glyceraldehyde-3-phosphate; AMP, adenosine monophosphate; DHAP, dihydroxyacetone phosphate; FBP, fructose-1,6-bisphosphate; 3/2PG, 3-phosphoglycerate & 2-phosphoglycerate; PEP, phosphoenolpyruvate; ADP, adenosine diphosphate; 6PG, 6-phosphogluconate; ATP, adenosine triphosphate; G6P, glucose-6-phosphate; F6P, fructose-6-phosphate; Ac-CoA, acetyl-Coenzyme A; GP, glucose-1-phosphate; NAD^+, oxidised nicotinamide adenine dinucleotide (NAD); NADH, reduced NAD; $NADP^+$, oxidised NAD phosphate (NADP); NADPH, reduced NADP; Succ., succinate; Fum., fumarate; Mal., malate; AKG, α-ketoglutarate; Cit., citrate; Pyr., pyruvate; Lac., lactate.

Figure 3. Individual principal component analyses of four time points for the metabolites analysed by LC-MS/MS. These time-points were chosen to demonstrate the rapid (< 5 min) but reversible (< 240 min) response to indole addition, which outweighed the differences between the wild-type and *hns*Δ93 strains. Points represent individual fermentations (n = 4) and ellipses represent 95% confidence intervals. The full series of PCA analyses for LC-MS/MS and GC-MS data are shown in Supplementary Fig. 1 and 2.

Figure 4. Overview of changes in central carbon metabolism in quiescent *E. coli* at 240 min. The color of each metabolite name corresponds to the average mean-centered fold change in concentration (n = 4) at the end of the time-course experiment for quiescent cultures (*hns*Δ93 with 3 mM indole). Metabolites in grey, underlined text had concentrations below the limit of detection. Those in black text were not possible to detect with our system.

Figure 5. Production summary of fed-batch cultures of *E. coli* W3110*hns*Δ93 producing 3HB, with or without the addition of indole (2.5 mM). As cells enter quiescence their metabolic effort is diverted away from biomass production and can be harnessed for the production of 3HB by metabolic pathway engineering. We show here the results of the experiment in which 2.5 mM indole was used. Similar results were achieved with other indole concentrations but are not directly comparable. **a**, Indole addition

(arrows) caused the culture to become quiescent within 2 h. **b**, Cumulative 3HB production following induction with IPTG (arrow heads). While the quiescent culture remained productive, the control stopped producing 3HB upon entry into stationary phase. **c**, Glucose utilisation rates were the same for both strains throughout the experiment. **d**, Specific 3HB formation rates (q_p) were initially the same, but reduced in the control during stationary phase.

Figure 1

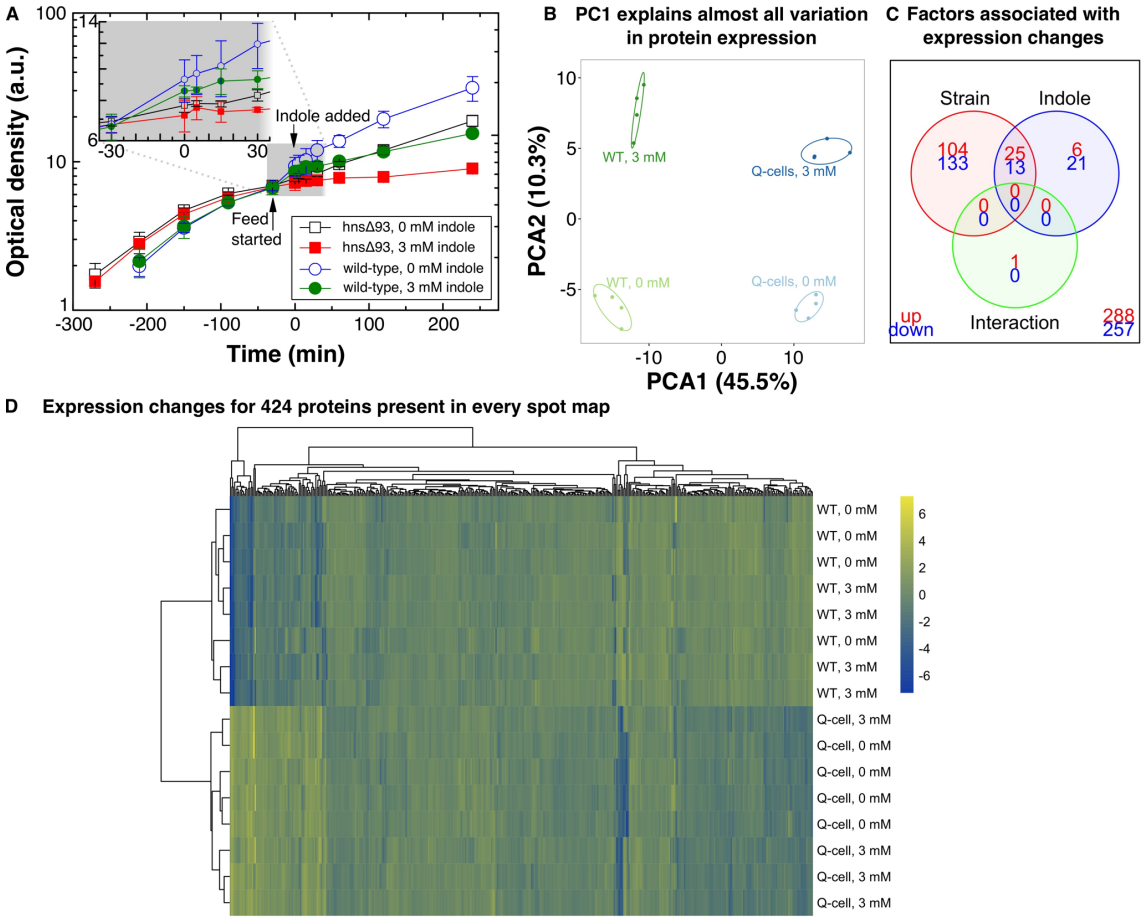
A
Optical density (a.u.)
Time (min)
Indole added
Feed started
hnsΔ93, 0 mM indole
hnsΔ93, 3 mM indole
wild-type, 0 mM indole
wild-type, 3 mM indole
B PC1 explains almost all variation in protein expression
PCA2 (10.3%)
PCA1 (45.5%)
WT, 3 mM
Q-cells, 3 mM
WT, 0 mM
Q-cells, 0 mM
C Factors associated with expression changes
Strain
Indole
Interaction
up
down
104
133
25
13
6
21
0
0
0
0
0
0
1
0
288
257
D Expression changes for 424 proteins present in every spot map
WT, 0 mM
WT, 0 mM
WT, 0 mM
WT, 3 mM
WT, 3 mM
WT, 0 mM
WT, 3 mM
WT, 3 mM
Q-cell, 3 mM
Q-cell, 0 mM
Q-cell, 0 mM
Q-cell, 0 mM
Q-cell, 0 mM
Q-cell, 3 mM
Q-cell, 3 mM
Q-cell, 3 mM

Figure 2

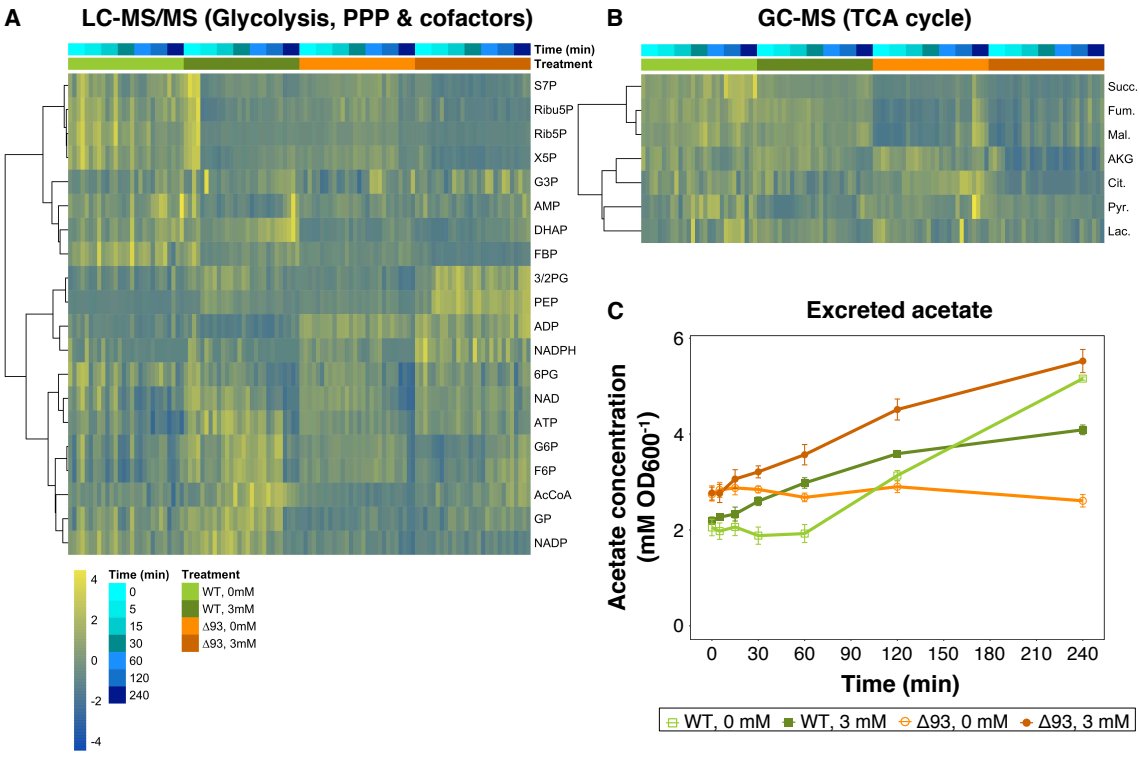
A
LC-MS/MS (Glycolysis, PPP & cofactors)
Time (min)
Treatment
S7P
Ribu5P
Rib5P
X5P
G3P
AMP
DHAP
FBP
3/2PG
PEP
ADP
NADPH
6PG
NAD
ATP
G6P
F6P
AcCoA
GP
NADP
4
2
0
-2
-4
Time (min)
0
5
15
30
60
120
240
Treatment
WT, 0mM
WT, 3mM
Δ93, 0mM
Δ93, 3mM
B
GC-MS (TCA cycle)
Succ.
Fum.
Mal.
AKG
Cit.
Pyr.
Lac.
C
Excreted acetate
Acetate concentration (mM OD600-1)
6
4
2
0
0
30
60
90
120
150
180
210
240
Time (min)
WT, 0 mM
WT, 3 mM
Δ93, 0 mM
Δ93, 3 mM

Figure 3

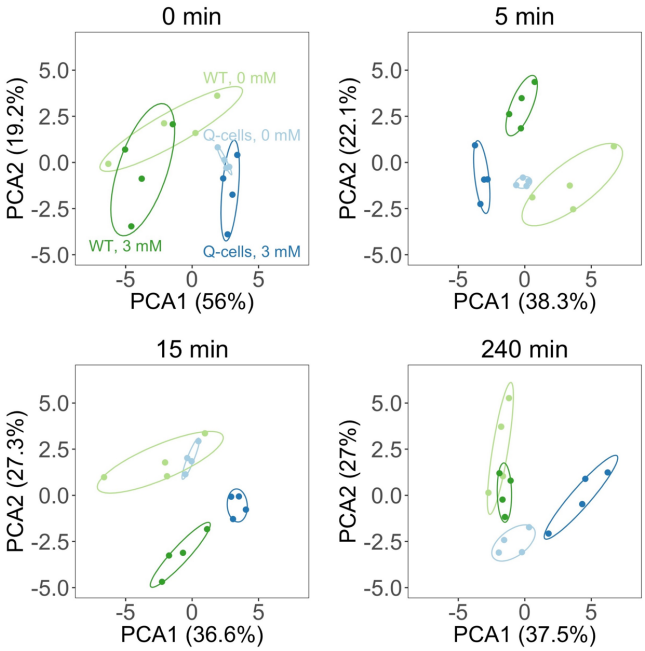
0 min
5 min
15 min
240 min
WT, 0 mM
Q-cells, 0 mM
WT, 3 mM
Q-cells, 3 mM
PCA1 (56%)
PCA2 (19.2%)
PCA1 (38.3%)
PCA2 (22.1%)
PCA1 (36.6%)
PCA2 (27.3%)
PCA1 (37.5%)
PCA2 (27%)
5.0
2.5
0.0
-2.5
-5.0
-5
0
5

Figure 4

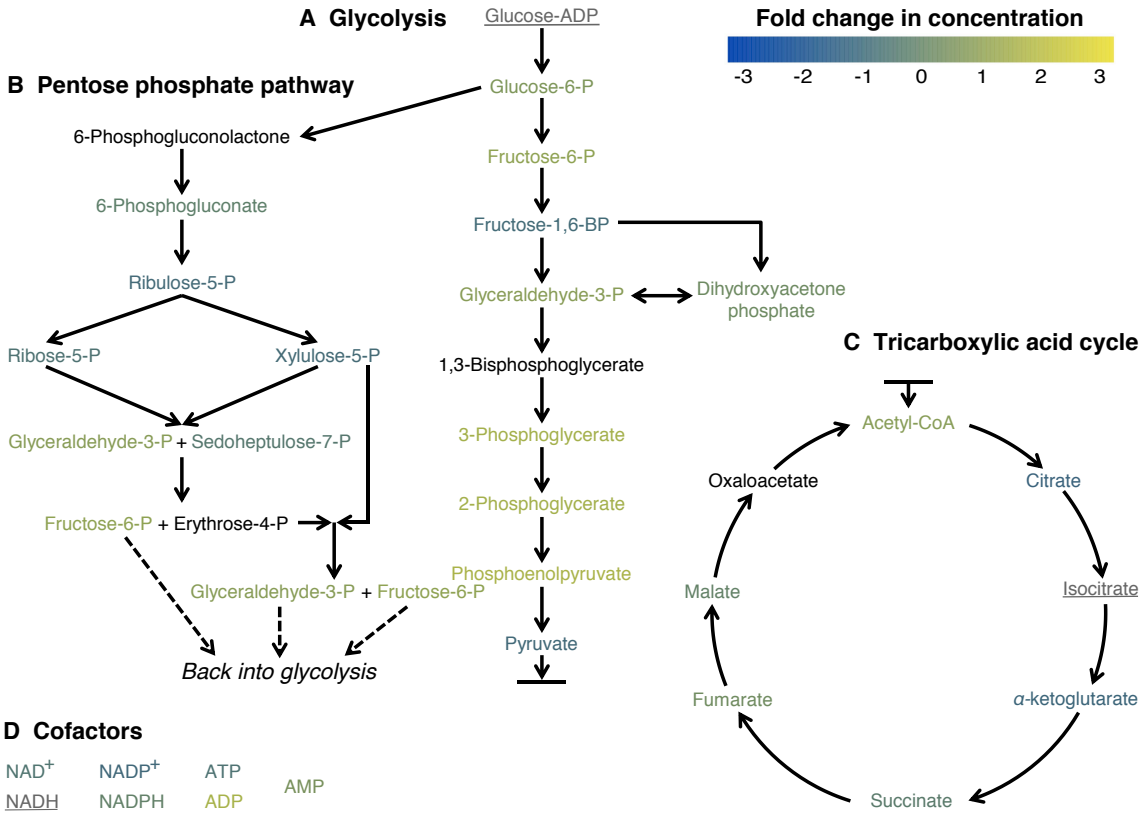
A Glycolysis
Glucose-ADP
Glucose-6-P
Fructose-6-P
Fructose-1,6-BP
Glyceraldehyde-3-P
Dihydroxyacetone phosphate
1,3-Bisphosphoglycerate
3-Phosphoglycerate
2-Phosphoglycerate
Phosphoenolpyruvate
Pyruvate
B Pentose phosphate pathway
6-Phosphogluconolactone
6-Phosphogluconate
Ribulose-5-P
Ribose-5-P
Xylulose-5-P
Glyceraldehyde-3-P + Sedoheptulose-7-P
Fructose-6-P + Erythrose-4-P
Glyceraldehyde-3-P + Fructose-6-P
Back into glycolysis
Fold change in concentration
-3 -2 -1 0 1 2 3
C Tricarboxylic acid cycle
Acetyl-CoA
Citrate
Isocitrate
α-ketoglutarate
Succinate
Fumarate
Malate
Oxaloacetate
D Cofactors
NAD+ NADP+ ATP
NADH NADPH ADP
AMP

Figure 5

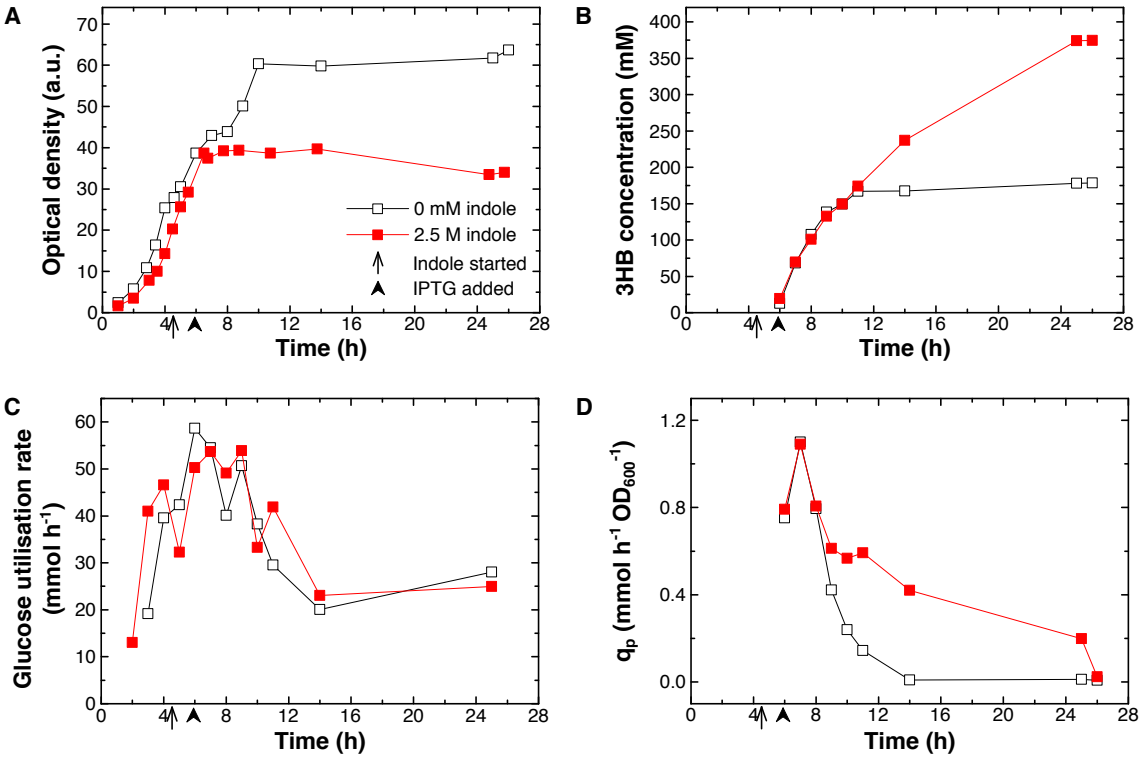
A
Optical density (a.u.)
Time (h)
0 mM indole
2.5 M indole
Indole started
IPTG added
B
3HB concentration (mM)
Time (h)
C
Glucose utilisation rate (mmol h-1)
Time (h)
D
qp (mmol h-1 OD600-1)
Time (h)